molecules

MDPI

Article

Reactive Molecular Dynamics Study of Pollutant Formation Mechanism in Hydrogen/Ammonia/Methanol Ternary Carbon-Neutral Fuel Blend Combustion

Jingyun Sun [1], Qianqian Liu [1], Yang Wang [1,2,*], Mingyan Gu [1] and Xiangyong Huang [1]

[1] School of Energy and Environment, Anhui University of Technology, Ma'anshan 243002, China; jingyunsun133@163.com (J.S.); liuqianqian208dw@163.com (Q.L.); gumy@ahut.edu.cn (M.G.); huangxy@ahut.edu.cn (X.H.)
[2] School of Materials Science and Engineering, Anhui University of Technology, Ma'anshan 243032, China
* Correspondence: wangyang@ahut.edu.cn; Tel.: +86-05552311816

Abstract: Hydrogen, ammonia, and methanol are typical carbon-neutral fuels. Combustion characteristics and pollutant formation problems can be significantly improved by their blending. In this paper, reactive molecular dynamics were used to investigate the pollutant formation characteristics of hydrogen/ammonia/methanol blended fuel combustion and to analyze the mechanisms of CO, CO_2, and NO_X formation at different temperatures and blending ratios. It was found that heating can significantly increase blending and combustion efficiency, leading to more active oxidizing groups and thus inhibiting N_2 production. Blended combustion pollutant formation was affected by coupling effects. NH_3 depressed the rate of CO production when CH_4O was greater than 30%, but the amount of CO and CO_2 was mainly determined by CH_4O. This is because CH_4O provides more OH, H, and carbon atoms for CO and CO_2 to collide efficiently. CH_4O facilitates the combustion of NH_3 by simplifying the reaction pathway, making it easier to form NO_X.

Keywords: carbon-neutral fuel; ternary blend combustion; NO_X; ReaxFF MD

Citation: Sun, J.; Liu, Q.; Wang, Y.; Gu, M.; Huang, X. Reactive Molecular Dynamics Study of Pollutant Formation Mechanism in Hydrogen/Ammonia/Methanol Ternary Carbon-Neutral Fuel Blend Combustion. *Molecules* **2023**, *28*, 8140. https://doi.org/10.3390/molecules28248140

Academic Editor: Hristiyan A. Aleksandrov

Received: 24 November 2023
Revised: 12 December 2023
Accepted: 15 December 2023
Published: 17 December 2023

1. Introduction

Currently, the global transportation industry relies mainly on fossil energy sources [1], but the combustion of these traditional fossil energy sources causes a lot of pollution. To fundamentally solve this problem, finding clean energy sources that can replace traditional energy sources has become one of the most important research topics [2,3].

H_2 and NH_3 are both ideal clean and renewable fuels that have received a lot of attention from scholars at home and abroad. H_2 can be produced renewably from green energy by electrolyzing water. In addition, it is characterized by good combustibility, low ignition energy, and fast combustion rates [4,5]. However, difficulties in storage and transportation, its excessive combustion rate, and its high combustion temperature producing NO_X pollution have limited the practical promotion of pure H_2 fuel use [6]. NH_3, as a good zero-carbon H_2 storage carrier, can be obtained from fossil fuels, biomass, or other renewable sources. This is why NH_3 has received a great deal of attention from the combustion community in recent years and is considered a sustainable fuel that can be remotely transported and applied [7]. NH_3 is currently used as a fuel in a wide range of applications, such as vehicle engines [8], marine engines [9], and combustion engines for power generators [10]. The low viscosity of NH_3 helps in fuel atomization and droplet formation during fuel injection [11]. In addition, NH_3 has a high octane rating, which makes it suitable for engines with high compression ratios and reduced detonation [12]. However, NH_3 has the disadvantages of a low combustion rate [13], high autoignition temperature [14], and narrow flammability limits, often leading to incomplete combustion. This contributes to poor engine performance, making it difficult to use as a single fuel

for direct combustion [15,16]. The use of H_2 as a combustion aid and NH_3 blending has been found to be one of the ways to improve the efficiency of NH_3 combustion [17]. This not only leads to improved in-cylinder combustion [18] but also reduces the requirement for engine modifications (material compatibility), thus ensuring a cost-effective transition to H_2 [19]. Wang et al. [20] found that engine exhaust heat can crack some of the NH_3 into H_2 and nitrogen to provide energy, making this method much more maneuverable. However, a study by Alam et al. [21] pointed out that although H_2-NH_3 blending reduces carbon emissions, including CO, etc., in diesel internal combustion engines, incomplete fuel combustion and higher NO_X were observed.

Blending oxygenated fuels as combustion aids is also an effective way to improve combustion performance and pollutant emissions in diesel engines [22]. In a study of LPG-diesel- and CNG-diesel-fueled diesel engines using the high-cetane fuel diethyl ether, improved combustion was observed [23]. Wang et al. [24] performed numerical simulations of ethanol and diesel blends on their combustion and emission characteristics. It was found that ethanol/diesel blends significantly reduced CO_2 and soot emissions compared to diesel. Soot and CO_2 emissions were reduced by 63.25% and 17.24% respectively at 100% load, but Nox was increased by 1.39%. Feng et al. [25] analyzed a methanol/diesel/n-butanol replacement blend. The results show that the thermal efficiency and the blending efficiency of diesel and alcohol fuel increase with an increase in the alcohol fuel blending ratio (0–15%), and irreversible loss also increases. Increasing the load on a diesel engine can improve its thermal efficiency. Wang et al. [26] investigated DGE as an oxygenated fuel and combustion enhancer to improve the combustion emissions of NH_3 and H_2 blends. It was found that when 60–70% of diesel fuel was replaced with DGE, H_2, and NH_3, CO_2 was reduced by 50% and synergistic effects were found between DGE and H_2 and NH_3, reducing PM, NO_X, HC, and CO emissions.

CH_4O, as the saturated monohydric alcohol with the simplest structure, is inexpensive and simple to synthesize. It is a high-quality representative for the study of combustion-enhancing effects on oxygenated fuels. Li et al. [27] found that blending a small amount of CH_4O into NH_3 combustion made the blend more reactive, due to the enrichment of the O/H radical pool by the addition of CH_4O. Species in this sequence can also react directly with NH_3 combustion-associated species, thereby consuming NH_3 and promoting spontaneous combustion. Xu et al. [28] simulated the combustion characteristics of NH_3/CH_4O blends and found that CH_4O makes a significant contribution to the laminar combustion rate of NH_3, and NO_X emission analysis showed that the blending of 60% CH_4O leads to the highest NO_X emissions. Lu et al. [29] investigated the effect of CH_4O doping on NH_3 combustion and emissions by modeling the chemical reaction mechanisms of an NH_3/CH_4O blend. The results showed that CH_4O doping significantly increased the chemical reaction activity of NH_3 and significantly reduced the ignition delay time.

Because of the complexity of the engine in cylinder combustion and its pollutant formation characteristics, it is not favorable to explore the chemical reaction kinetics and blended fuel combustion pollutant laws under different operating parameters in isolation [30,31]. In this paper, CH_4O is used as a representative of oxygenated fuels. Reactive molecular dynamics are used to investigate the effect of CH_4O on the combustion pollutant formation characteristics of H_2 and NH_3 combustion-reforming gases in diesel engines. This study analyzes the pollutant formation mechanisms of CO, CO_2, and NO_X formations at different temperatures and fuel ratios at the molecular level. This study is of great theoretical and practical significance to enhance the application of carbon-neutral fuels in engines and other practical combustion equipment.

2. Results and Discussion

2.1. Temperature Effects on Ternary Blended Combustion Components and Pollutant Formation

2.1.1. Temperature Effects on Ternary Blended Combustion Components and Free Radicals

Figure 1 shows the effects of different temperatures on the four reactant components CH_4O, NH_3, H_2, and O_2 in the ternary blended combustion process. From the figure,

it can be seen that heating significantly accelerated the decomposition rate of CH_4O, NH_3, H_2, and O_2. The insignificant rises for H_2 and O_2 at high temperatures may be caused by the decomposition of H_2O due to the intensification of molecular collisions at high temperatures.

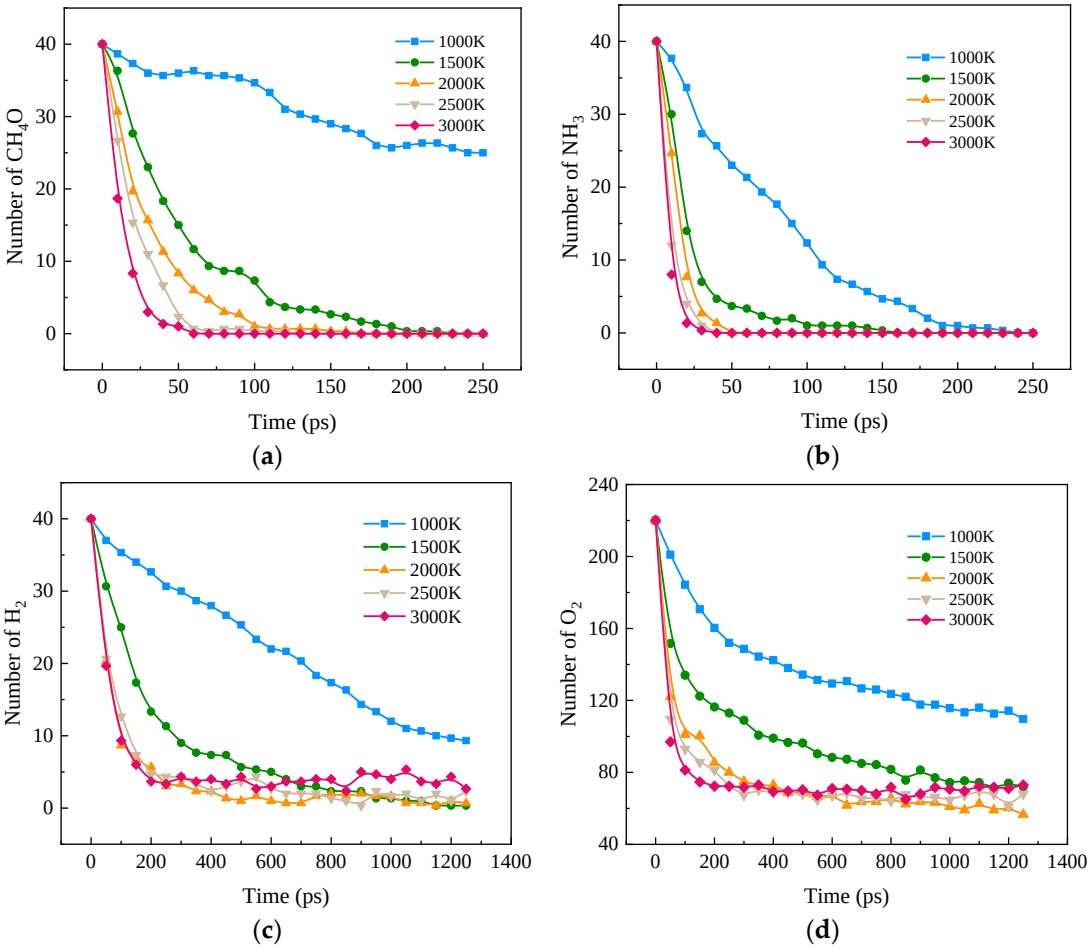

Figure 1. Changes in reactants during the combustion of carbon-neutral fuels at different temperatures. (**a**) CH_4O; (**b**) NH_3; (**c**) H_2; (**d**) O_2.

Figure 2a,b shows the effects of different temperatures on the formation of H_2O and N_2 in the combustion process. From Figure 2a, it can be seen that the growth rate of H_2O slows down significantly after a rapid increase to a certain level. Heating accelerates the rate of H_2O formation during combustion. However, the effect of heating is not obvious when the temperature is further increased above 2000 K. Above 2500 K, H_2O shows an insignificant decreasing trend, which may be due to the decomposition of H_2O at high temperatures. This conclusion is consistent with the above conclusion that high temperatures lead to a slowly increasing trend for H_2 and O_2 at the late stage of the reaction. In Figure 2b, it is visible that the variation rule for N_2 at different temperatures is not strictly temperature-dependent. The maximum amount of N_2 generated by the reactants is at 1000 K. Above 2500 K and 1500 K, the amount of N_2 generated increases with an increase in temperature. However, in the case of 2000 K, the amount of N_2 is significantly lower than for other temperatures. This is because N from NH_3 generates more NO_X at 2000 K.

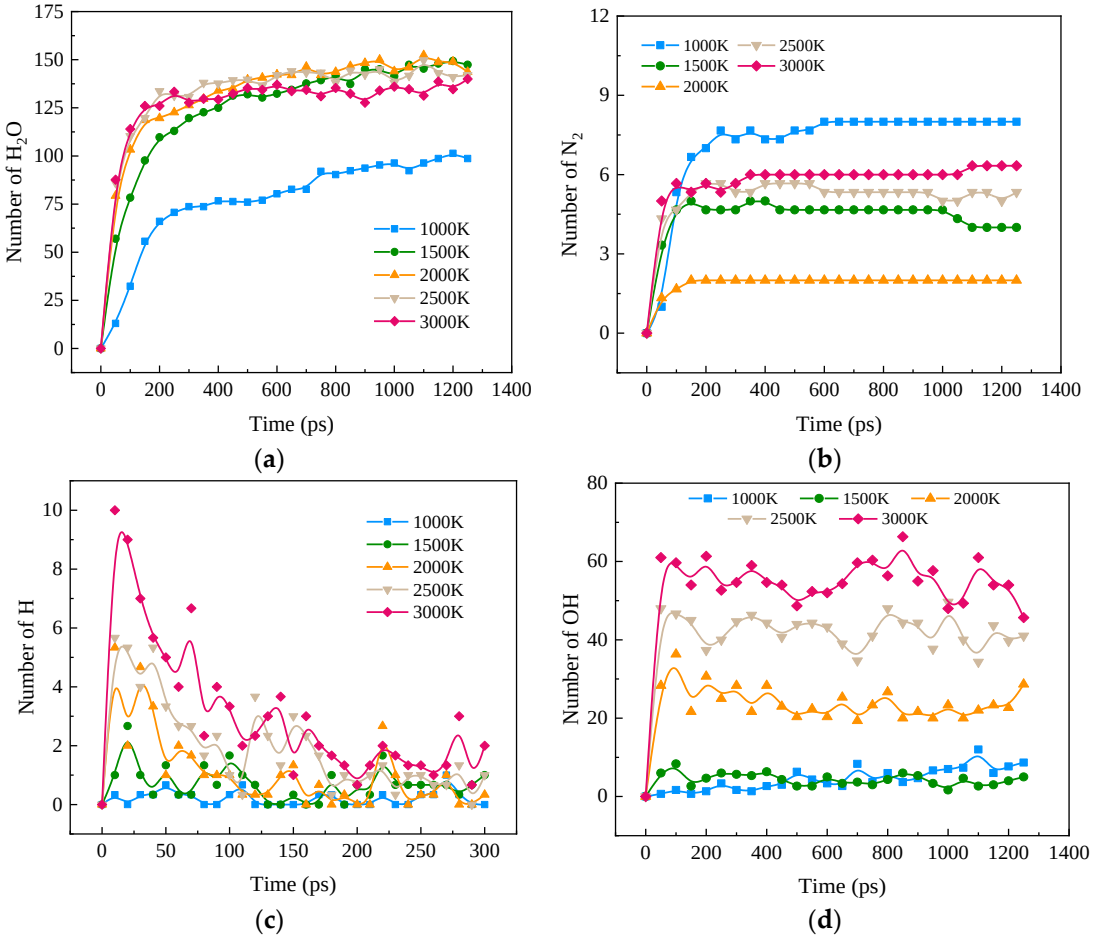

Figure 2. Changes in components and radicals during combustion at different temperatures. (**a**) H_2O; (**b**) N_2; (**c**) H; (**d**) OH.

Figure 2c,d shows the effects of different temperatures on the formation of H and OH during blended combustion. It can be seen that the formation of H and OH is slow at low temperatures and the quantity is depleted as the reaction continues. High temperatures increase the amounts of H and OH. The difference is that H peaks rapidly and then decreases as the reaction proceeds, while OH peaks and then stabilizes as the reaction proceeds. The peak H at 3000 K is five times higher than that at 1500 K. Heating significantly increases the H and OH concentrations in the combustion reaction.

2.1.2. Temperature Effects on CO and CO_2 Formation in Blended Combustion

Figure 3a,b shows CO and CO_2 formation during the blended combustion process at different temperatures. Heating increases the rate of CO production, where CO is formed rapidly and then decreases slowly at temperatures of 2000 K and higher. At 1500 K and 1000 K, CO has still not peaked at the end of the reaction and is in a state of continuous growth. As the temperature increases the CO_2 production rate increases, and the peak state remains almost stable. However, some of the CO is further oxidized to CO_2 at high temperatures. Heating significantly accelerates the production of CO and CO_2. The decrease in CO_2 at 3000 K is because the high temperature promotes the reduction of more CO_2 to CO.

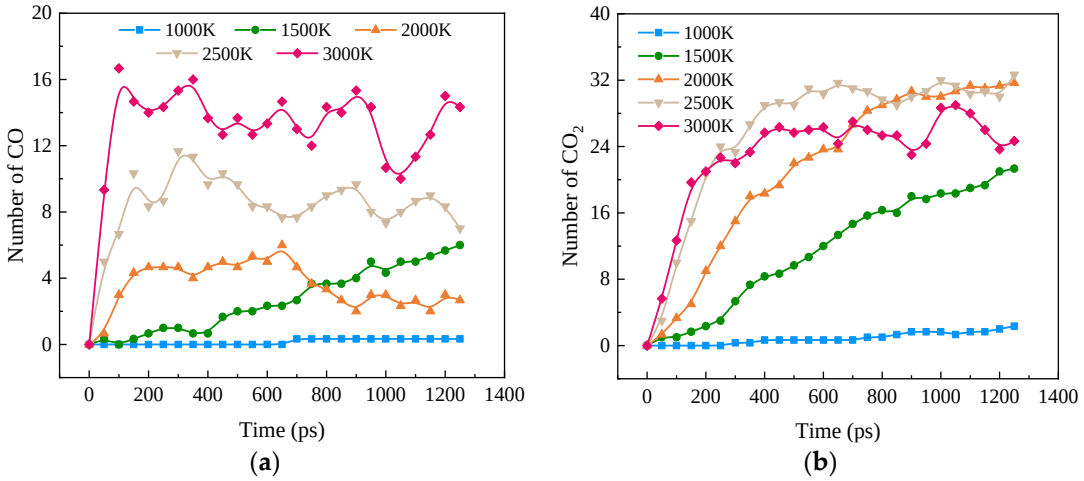

Figure 3. CO and CO_2 formation with time for blended combustion at different temperatures (**a**) CO; (**b**) CO_2.

2.1.3. Temperature Effects on NO_X Formation from the Blended Combustion of Ternary Carbon-Neutral Fuels

Figure 4 shows the effects of temperature on the formation of NO_X (NO, NO_2, and NO_3) in the combustion of ternary carbon-neutral fuel blends. From Figure 4a, it can be seen that, as the reaction proceeds, NO is first generated rapidly. NO at low temperatures is gradually depleted after reaching the peak value, but the amount of NO at high temperatures is relatively stable. As the temperature increases, the NO peak is gradually shifted forward, and the peak value increases.

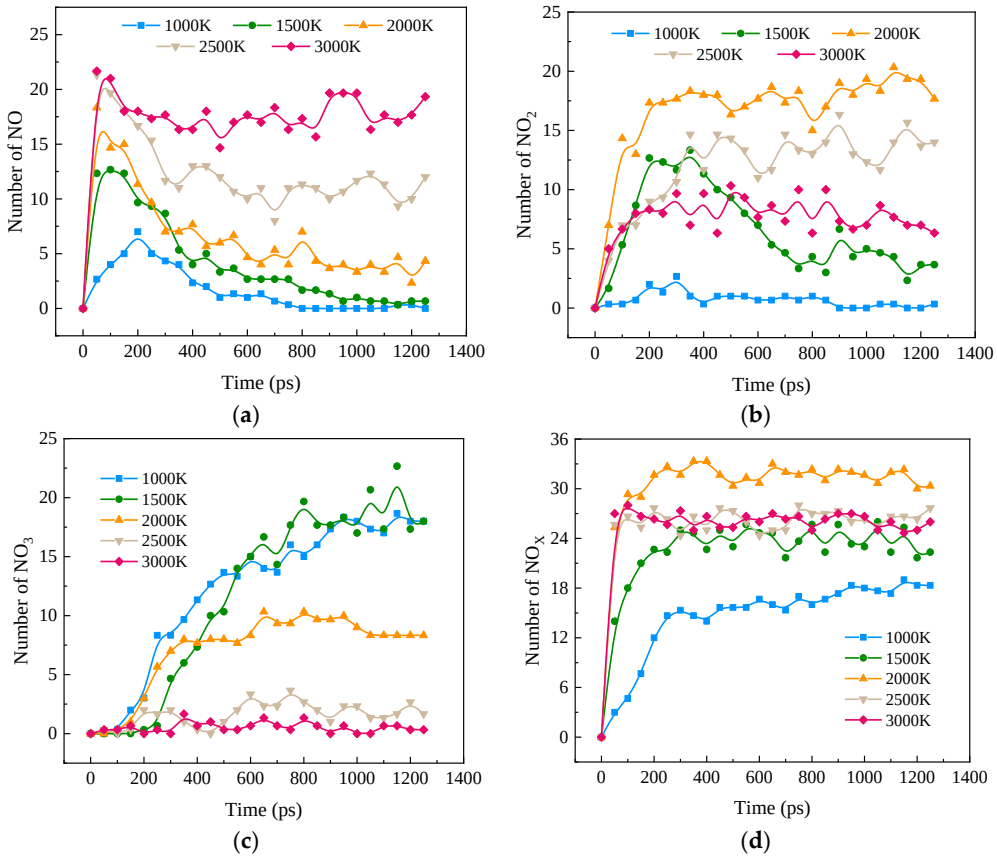

Figure 4. Distribution of NO_X during the combustion of ternary carbon-neutral fuel blends. (**a**) NO; (**b**) NO_2; (**c**) NO_3; (**d**) NO_X.

Figure 4b shows the change in NO_2 with combustion, and its change rule in the range of 2000 K to 3000 K is opposite to that of NO, in which the largest amount of NO_2 exists at 2000 K, followed by 2500 K, with the least at 3000 K, which may be caused by part of NO_2 being reduced at a high temperature. NO_2 at 1500 K shows the same trend of increasing and then decreasing as NO in this condition. The time of peak NO coincides with the time of a rapid increase in NO_2, and the time of a large amount of NO consumption coincides with the time of peak NO_2, so the consumed NO_2 is further oxidized to NO_3.

Figure 4c represents the variation in NO_3 as the combustion reaction proceeds, with almost no change for the two high-temperature conditions. Its rise at 2000 K is followed by a steady rise and a rapid and sustained rise in the low-temperature condition.

Figure 4d represents the rapid formation and gradual stabilization of NO_X as the blended combustion reaction proceeds. The effect of heating on the NO_X peak is nonlinear. The NO_X peak growth rate slows down with increasing temperature and reaches a peak at 2000 K. The NO_X peak growth rate is also shown in Figure 4d, which shows that NO_X formation is rapid and stabilizes under ternary combustion.

Heating accelerates the formation of NO_X, but high temperature inhibits the formation of NO_X when the temperature is higher than 2000 K. At low temperatures, NO_X exists mainly in the form of NO_3. At high temperatures, the main form of NO_X is NO. At 2000 K, NO_2 is the main form of NO_X. This is probably because high temperature accelerates the reduction of NO_X.

2.2. Influence of Blending Ratio on Combustion Composition and Pollutant Formation

2.2.1. Influence of Blending Ratio on Combustion Components and Free Radicals

A comparison and analysis of different blending ratios were carried out to obtain the formation patterns of reactants and NO_X in ternary blended combustion under different blending ratios. Figure 5 shows the changes in reactants with time under different blending ratios. When the proportion of CH_4O is more than 30%, the lower the proportion of NH_3, the faster and more complete the reaction. When the proportion of CH_4O is less than 30%, the reaction rate of CH_4O is faster in the case of H_2/NH_3 being more than 1, which is because H_2 promotes the decomposition of CH_4O. Therefore, NH_3 inhibits CH_4O combustion and H_2 promotes CH_4O combustion in blended fuel combustion. When the proportion of CH_4O is more than 30%, NH_3 plays a major role. When the proportion of CH_4O is less than 30%, H_2 plays a major role.

As shown in Figure 5b, the higher the CH_4O percentage, the higher the NH_3 reaction rate and the more complete the reaction. When the amount of NH_3 is determined, the working NH_3 reaction rate is faster for CH_4O/H_2 greater than 1. This is because CH_4O can promote the combustion of NH_3. As shown in Figure 5c, the lower the NH_3 percentage the higher the H_2 reaction rate and the more complete the reaction. This is because NH_3 inhibits H_2 combustion. When the amount of H_2 is determined, the H_2 reaction rate is faster for the working condition of CH_4O/NH_3 greater than 1, which also indicates that NH_3 inhibits H_2 combustion during the combustion of blended fuels.

From Figure 6a, it can be seen that the growth rate of H_2O slows down significantly after a rapid rise to a certain level. With the increase in the proportion of H_2, the rate of H_2O generation is accelerated, and it can be seen that H_2 accelerates the rate of H_2O formation in the combustion process. Through Figure 6b, it can be found that with the reaction, N_2 rises rapidly to a certain degree and then stabilizes, and N_2 rises with an increase in NH_3 content under different doping ratios. Because H_2 and NH_3 have a competitive relationship in the combustion process, and N_2 is a product of NH_3 combustion, when NH_3 is the same, the smaller the proportion of H_2 the faster N_2 rises and the larger the peak. However, in the case of a $H_2/NH_3/CH_4O$ ratio of 1:2:3, the amount of N_2 is significantly lower than a ratio of 3:2:1, which may be due to the large amount of CH_4O affecting the conversion of NH_3 to N_2 during combustion, which will be further verified at the molecular level in Section 3.4.

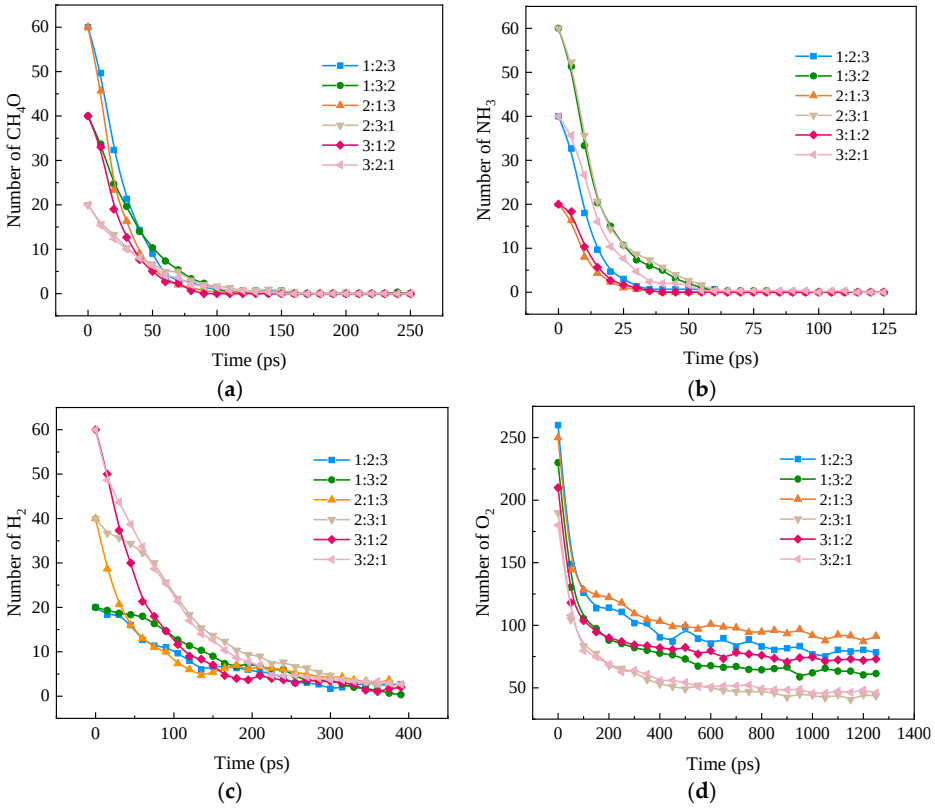

Figure 5. Changes in reactants in the combustion process of ternary carbon-neutral fuel blends with different blending ratios. (**a**) CH_4O; (**b**) NH_3; (**c**) H_2; (**d**) O_2.

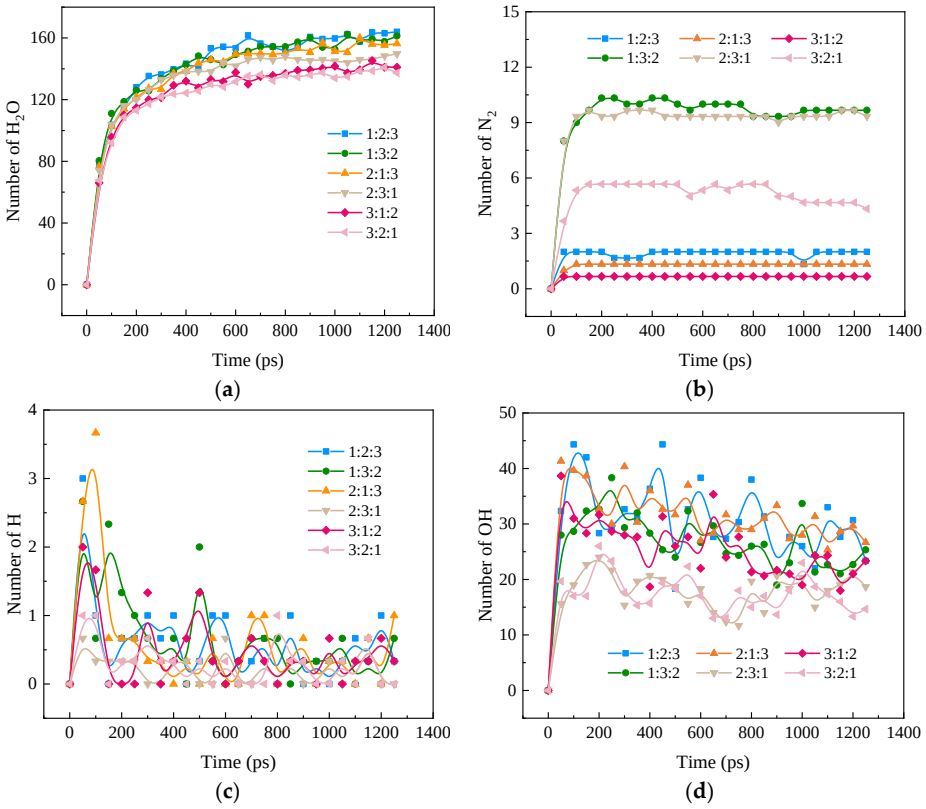

Figure 6. Variation in combustion components and free radicals in ternary carbon-neutral fuel blends with time at different blending ratios. (**a**) H_2O; (**b**) N_2; (**c**) H; (**d**) OH.

Figure 6c,d, on the other hand, shows the effect of different blending ratios on the formation of H and OH during the ternary hybrid combustion. It can be seen that H shows an increasing and then decreasing trend as the reaction proceeds. The conclusion is that the peak H value increases with increasing CH_4O percentage. When the proportion of CH_4O in the blending fuel remains constant, H_2 has a certain promotion effect on H peak generation, and NH_3 has a certain inhibition effect. When the proportion of CH_4O is more than half, the inhibitory effect is greater than the promotion effect, and OH grows to the peak and then decreases slowly as the reaction, which is almost stable, proceeds. The peak rises with the increase in CH_4O percentage. When the proportion of CH_4O in the blending fuel remains constant, unlike H, NH_3 promotes the generation of OH while H_2 inhibits it, and the inhibitory effect is greater than the promotional effect when the proportion of H_2 is more than half. Therefore, the concentration of radicals H and OH in the ternary blended combustion reaction is mainly affected by CH_4O.

2.2.2. Influence of the Blending Ratio on CO and CO_2 Formation in Blended Combustion

Figure 7a,b shows CO and CO_2 formation during the ternary fuel blending process at different blending ratios, respectively. As the CH_4O combustion reaction proceeds, the rate of CO formation is mainly affected by NH_3, which slows down the rate of CO formation at a CH_4O share of more than 30%. However, the amount of CO production is mainly influenced by CH_4O, which increased with the increase in CH_4O percentage. When the proportion of CH_4O in the blending fuel remains constant, the larger the proportion of H_2, the larger the peak of CO, which may be due to the combustion process of H_2 to promote the production of CO. CO_2, in the progress of the reaction, shows a continuous increase in the trend of the rate, and the amount of CO_2 production is mainly affected by the proportion of CH_4O. When the proportion of CH_4O in the blending fuel remains constant, the higher the proportion of H_2, the faster the reaction, and the greater the amount of formation, indicating that H_2 plays a role in promoting the formation of CO_2, while NH_3, and CH_4O have a competitive relationship.

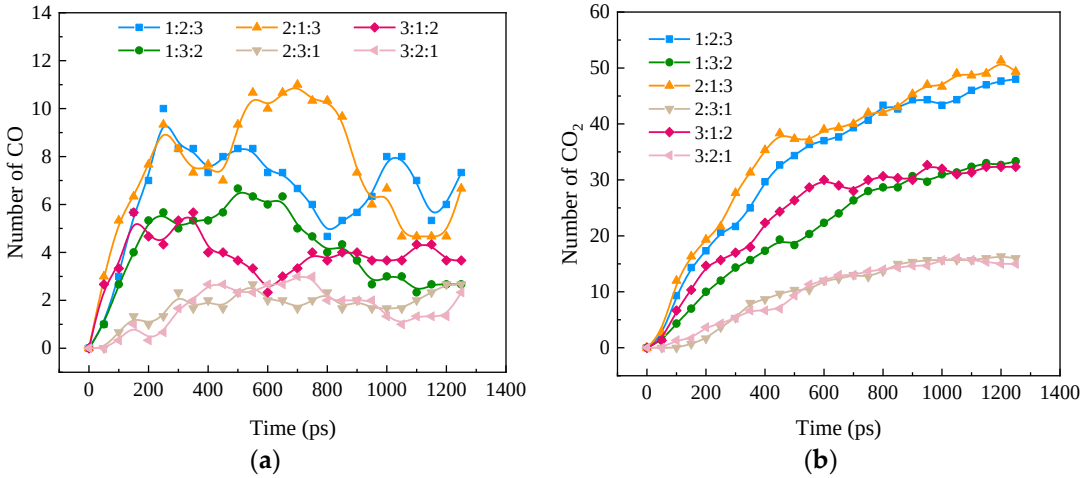

Figure 7. CO and CO_2 formation over time for blended combustion at different blending ratios (**a**) CO; (**b**) CO_2.

In summary, it is shown that the production of CO and CO_2 during the combustion of a blend of ternary carbon-neutral fuels is not simply influenced by CH_4O alone but is a result of the coupling of three fuels, H_2, NH_3, and CH_4O, which will be examined on a molecular level in a detailed pathway analysis in Section 3.4.

2.2.3. Influence of Blending Ratio on NO_X Formation in Blended Combustion

Figure 8 shows the influence of the NH_3 blending ratio on the formation of NO_X (NO, NO_2, and NO_3) during the blended combustion of ternary carbon-neutral fuels. Figure 8a

shows that, as the reaction proceeds, NO is first generated rapidly and then gradually depleted. The NO formation rates and the peak values are in the ratios 2:3:1, 1:3:2, 1:2:3, 3:2:1, 2:1:3, and 3:1:2 from large to small, respectively. The time of peak appearance is positively correlated with the size of the peaks. The rate of NO formation and the magnitude of the peak are mainly influenced by NH_3 in the fuel blends. When NH_3 is quantized, CH_4O promotes NH_3 combustion. Figure 8b represents the change in NO_2 with the combustion reaction process, and the NO_2 reaction fluctuates up and down around the peak value after a certain stage. The trend of the magnitude of the stabilization value with the blending ratio is similar to that of NO, and the rate of NO_2 formation and the magnitude of the peak are mainly affected by the NH_3 in the blended fuels. Comparing 1:2:3 and 3:2:1, it can be seen that CH_4O promotes the combustion of NH_3 but increases the formation of NO_2. Figure 8c represents the variation in NO_3 as the combustion reaction proceeds, showing a continuous growth trend as the reaction proceeds, but the growth rate is slow and then fast. The variation in the blending ratio is also similar to that of NO.

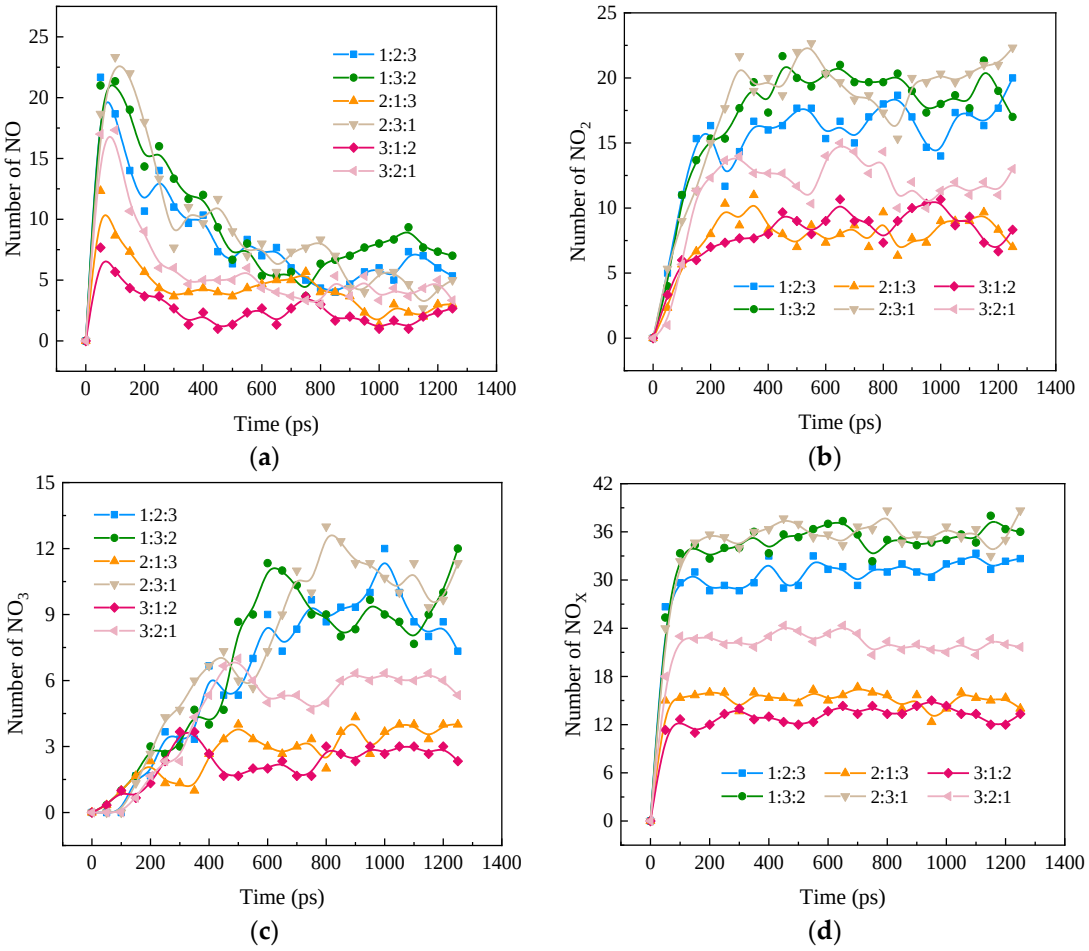

Figure 8. Distribution of NO_X during the combustion of ternary carbon-neutral fuel blends at different blending ratios. (**a**) NO; (**b**) NO_2; (**c**) NO_3; (**d**) NO_X.

Figure 8d shows the rapid formation and gradual stabilization of NO_X as the combustion reaction proceeds. As the NH_3 percentage increases, the NO_X peak increases. When NH_3 is quantized, the higher the CH_4O content, the higher the NO_X peak. Based on the NH_3 percentage, it was hypothesized that there should be little difference between the ratio of 1:2:3 and the ratio of 3:2:1 NO_X quantities, but the result was unexpected. The NO_X value of 1:2:3 was 25% higher than that of 3:2:1, which may be due to the fact that CH_4O increased the conversion rate of NH_3 to NO_X. In order to gain insight into the effects

of doping ratio on NO_X formation, reaction pathway analysis will be carried out at the molecular level in the following.

2.3. Analysis of the Mechanisms of CO, CO_2, and NO_X Formation in the Combustion of Blended Fuels as Affected by Temperature

This section will further discuss temperature-influenced ternary blended fuel combustion in the mechanism of CO, CO_2, and NO_X formation. In this section, the N and C migration paths during ternary blended fuel combustion simulated by ReaxFF MD at different temperatures are generated and discussed for Case 1, Case 2, and Case 5 as examples. Figure 9a–c represents the network diagrams for NO_X formation reaction paths during the combustion of ternary fuel at temperatures of 1000 K, 2000 K, and 3000 K. The percentages in the network diagrams indicate the reactant conversion rates. In order to highlight the main paths of the reaction network, reaction paths with a conversion rate of less than 15% are ignored in all network diagrams in this study.

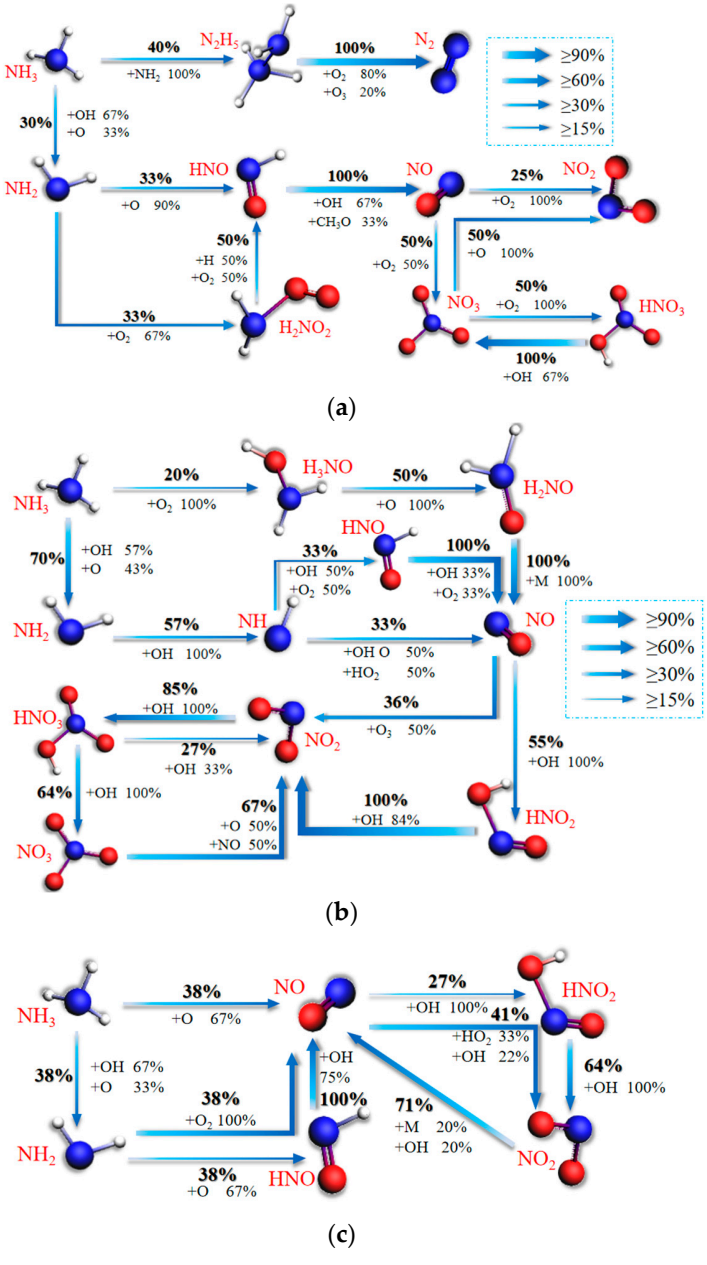

Figure 9. Mechanisms of NO_X formation from blended combustion at different temperatures. (**a**) 1000 K; (**b**) 2000 K; (**c**) 3000 K.

Comparative analysis of the graphs in Figure 9 reveals that the complexity of the paths appears to be greater and then lesser as the temperature increases; the paths are most complex at 2000 K. The complexity of the paths is greater when the temperature is too low. This may be because the reaction is incomplete and molecular activity is low at 1000 K. Therefore, many molecules do not have the opportunity to collide with each other, so there are fewer intermediate products and the path is simpler. At 3000 K, because of the high temperature, the reactants are very active, especially the O molecules, so that many reactions can occur in a very short period of time. The oxidation of NH_3 by OH during the conversion of NH_3 molecules to NH_2 decreases from 66.7% to less than 10%, but O increases rapidly from 33% to 67%. The intermediates required for the conversion of NH_3 molecules to NO are gradually reduced from three to direct oxidation without intermediates. Thus, higher temperatures significantly contribute to the NH_3 combustion reaction rate. By comparing Figure 9a–c, it is found that, as the temperature is further increased to 3000 K, the high temperature leads to the disappearance of the pathway for NH_3 to generate NiHi, which cannot generate N_2 but directly generates NO, and the significant increase in H and OH concentrations also contributes to the generation of NO from NH_3 to a certain extent. This analysis validates the conclusion in Section 3.1 of this paper about heating. Although accelerating the formation of NO_X is not conducive to the formation of NH_3, the conclusion is that high temperature inhibits NO_X formation when the temperature is higher than 2000 K. The results of this analysis are summarized in Figure 2c.

Analyzing the redox process for NO_X, it was found that NO_X is all formed by NO conversion. At low temperatures (1000 K), 50% of NO is oxidized directly to NO_3, while 25% of NO is oxidized to NO_2. A total of 50% of NO_3 can be reduced to NO_2, but NO_2 and NO_3 cannot be reduced directly to NO. Therefore, at low temperatures, NO_X exists mainly as NO_3. At 2000 K, the direct oxidation path from NO to NO_3 disappears, and it needs to pass through NO_2 to form NO_3. Overall, 91% of NO is oxidized directly or indirectly to NO_2, and the reduction of NO_3 to NO_2 is as high as 67%. Therefore, at 2000 K, NO_2 is the main form of NO_X. At high temperatures (3000 K), the pathway to generate NO_3 disappears, and 68% of NO is oxidized directly or indirectly to NO_2. The reduction rate for NO_2 is as high as 71%. Therefore, NO_X mainly exists in the form of NO at high temperatures.

Figure 10a–c represents the network diagrams of CO_2 formation reaction paths during combustion of ternary fuels at temperatures of 1000 K, 2000 K, and 3000 K. From Figure 10a, it can be found that 90% of CH_4O molecules first collide with OH from O_2 decomposition to form CH_3O. A total of 75% of CH_3O collides with HO_2 and O to form CH_2O, which is oxidized by O to form CH_2O_2. CH_2O_2 is oxidized by NO_2 and O to form CHO_2, which collides with OH to form CO_2. The reaction paths are chain-shaped in this case. The path is chain-shaped and has a simple structure.

Figure 10b represents the main reaction paths of CO and CO_2 formation by combustion of ternary hybrid fuel at a temperature of 2000 K. It can be seen that 73% of CH_4O molecules will collide to form CH_3O by the H_2 extraction reaction. CH_3O continues to collide with OH and O_2 to form CH_2O by a dehydrogenation reaction, while 27% of CH_4O is oxidized by O_2 to form CH_2O. Unlike at 1000 K, the path from CH_2O to CHO_2 has expanded by two pathways: 64% of CH_2O will collide with OH to form CHO first, and then collide with groups such as OH or H_2O to form CHO_2, while 18% of CH_2O collides directly with O to form CHO_2. The proportion of CH_2O_2 formation through collision with O to form CHO_2 and then CHO_2 (as at 1000 K) has decreased from 100% to 18%. CHO_2 collides with groups such as OH and O_2 to form CO_2. CO_2 is formed in the presence of groups such as OH, O_2, O, and so forth. CO and CO_3 ultimately flow to CO_2. CO_2 remains relatively stable in the form of an end product.

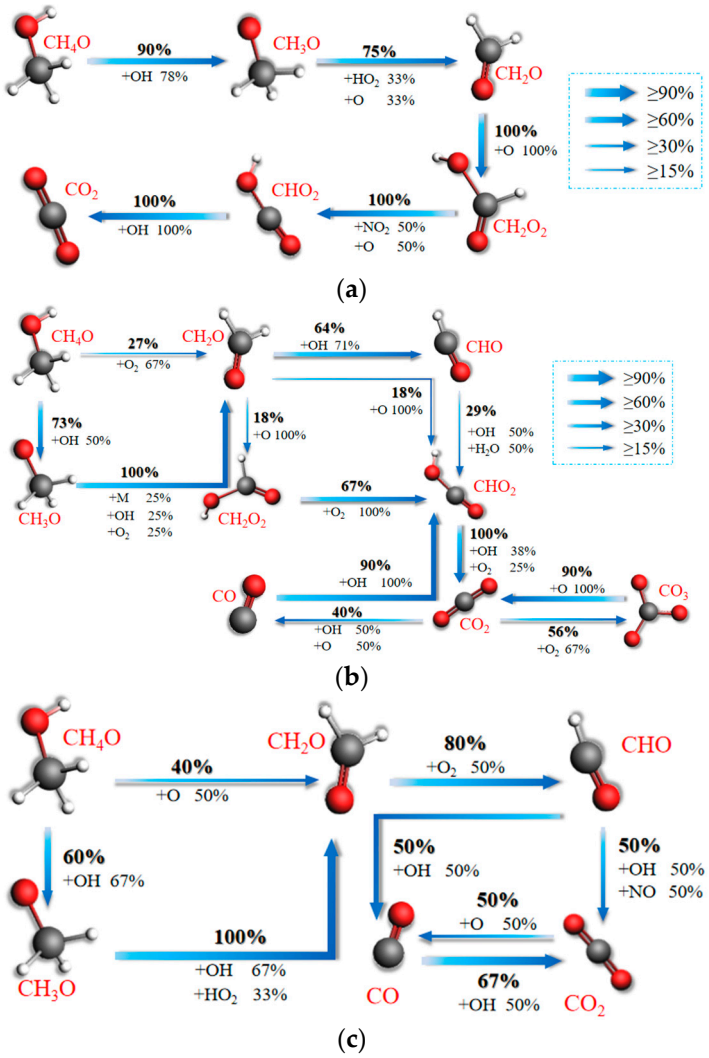

Figure 10. Mechanisms of CO and CO_2 formation in the blended combustion of ternary carbon-neutral fuels at different temperatures. (**a**) 1000 K; (**b**) 2000 K; (**c**) 3000 K.

Figure 10c shows the main reaction paths for CO_2 formation from the combustion of ternary hybrid fuels at a temperature of 3000 K. It is found that 60% of CH_4O reacts with OH to form CH_3O at the beginning of the combustion process at a temperature of 3000 K, and 40% of CH_4O is directly formed into CH_2O under the action of O. The proportions of CH_4O reacting with OH to form CH_3O at temperatures of 1000 K and 2000 K are 90% and 73%, respectively. The present reaction is only at 60%, and the proportions of CH_4O directly oxidized into CH_2O are 0 and 27% respectively, growing to 40% in the present case. Therefore, in this study, it was found that the oxidation of CH_4O molecules during the combustion of ternary blended fuels is more pronounced as the temperature increases. This is mainly due to the fact that as the temperature increases the ternary fuel combustion reaction contains more free OH and O. The temperature also means the reactant movement is more violent, allowing more molecules to collide and participate in the pyrolysis reaction. A temperature of 3000 K generated 80% of CH_2O by direct O oxidation to CHO; CHO and OH collision generated under half of the formation of CO and half of the formation of CO_2.

Through further comparative analysis, it was found that with an increase in temperature, as for the N migration path, the complexity of the C migration path appeared to become larger and then smaller. The path is most complex at 2000 K. The consumption of CH_4O molecules decreases the percentage of flow to CH_3O from 90% to 60%, a decrease of 30%. The proportion of flow to CH_2O increases from 0 to 40%, an increase of 40%.

Thus, higher temperatures significantly contribute to the NH_3 combustion reaction rate. By comparing Figure 10a–c, it is found that the percentage of CO formation is very small at low temperatures. At 2000 K, a CO formation pathway emerges from the reduction of 40% CO_2 and the combination of 90% of this with OH to form CHO_2. At a high temperature, unlike at low and medium temperatures, CO_2 is not the only source of CO, which is not only derived from 50% CO_2, but also from 50% CHO. In addition, the consumption of CO also decreases from 90% to 67%. Therefore, with further increases in temperature, the rate of CO and CO_2 formation rises, and the CO peak increases. Reaction path analysis explains the phenomenon in Section 3.1 of this paper that heating accelerates the rate of CO and CO_2 formation and the increase in peak CO with increasing temperature.

2.4. Mechanism and Reaction Path Analysis of CO, CO_2, and NO_X Formation in Blended Fuel Combustion as Affected by Blending Ratio

This section will further discuss the influence of blending ratio in the combustion of ternary blended fuel on the mechanisms of CO, CO_2, and NO_X formation. In this paper, the N and C migration paths of ternary blended fuel combustion are simulated by ReaxFF MD with different blending ratios generated and discussed for Case 1, Case 6, Case 7, and Case 9 as examples. Figure 11a–d represents the NO_X formation reaction path network diagrams during the combustion of ternary fuels with $H_2/NH_3/CH_4O$ blending ratios of 2:2:2, 1:2:3, 1:3:2, and 2:3:1.

From Figure 11a, it can be found that NH and H_3NO generate NO by oxidizing to produce HNO and H_2NO. A total of 55% of the NO collides with OH to produce HNO_2, whose continued collision with OH leads to the formation of NO_2. Meanwhile, 36% of NO is oxidized directly to NO_2. A total of 85% of the NO_2 collides with OH to produce HNO_3, and 64% of the HNO_3 is dehydrogenated to produce NO_3 before it is reduced to NO_2 by NO, while 27% of the HNO_3 is directly reduced back to NO_2 by collision with OH. A total of 25% of the NO_2 remains relatively stable in the form of an end product.

Figure 11b shows the main reaction pathways for the formation of NO_X from blended combustion with a ratio of 1:2:3. HNO is oxidized to NO by O_2, while 25% of NH is directly oxidized to NO by collision with OH. Subsequently, 14% of the NO remains relatively stable as an end product; 50% of the NO collides with OH to form HNO_2, which is then reduced to NO_2 by the continued collision with OH and O_2; 36% of the NO is directly oxidized to NO_2; and 38% of the NO is dehydrogenated with OH to form HNO_3. A total of 60% of the HNO_3 is dehydrogenated to NO_3 and then reduced to NO_2 by O. A total of 40% of HNO_3 is dehydrogenated to NO_3 before being reduced to NO_2 by O.

Figure 11c shows the main reaction paths of NO_X formation for blended combustion with a ratio of 1:3:2. A total of 37.5% of the NH_2 collides and combines with NH_2 groups to form N_2H_4. It continues to collide with groups such as OH, O_2, etc., to eventually form N_2. Meanwhile, 25% of the NH_2 collides with OH in a dehydrogenation reaction to form NH. NH collides with oxidizing groups such as O_2, HO_2, and O to form HNO. HNO collides with OH to form NO. A total of 12% of the NO remains relatively stable as an end product; 75.68% of the NO is oxidized to NO_2; 37% of the NO_2 combines with OH to form HNO_3. HNO_3 continues to collide with OH to form NO_3. A total of 44% of the NO_3 is reduced to NO_2 by groups such as O and OH, but HNO_3 is not the only source of NO_3. This is because 25% of NH_2 forms NO_3 through H_3NO as well.

Figure 11d represents the main reaction pathways for NO_X formation in blended combustion with a ratio of 2:3:1. HNO is oxidized to NO by groups such as HO_2 and OH. A total of 20% of the NH_2 collides with OH to form NH; 67% of the NH is oxidized directly to NO by groups such as O and O_2; 25% of the NH is oxidized directly to NO by collisions with OH. In total, 33% of the NO and of the OH produce NO_2 indirectly via HNO_2, while 42% of the NO is oxidized directly to NO_2. Overall, 22% of the NO_2 collides with OH to produce NO_3; 80% of the NO_3 is reduced directly back to NO_2 by collisions with O and NO.

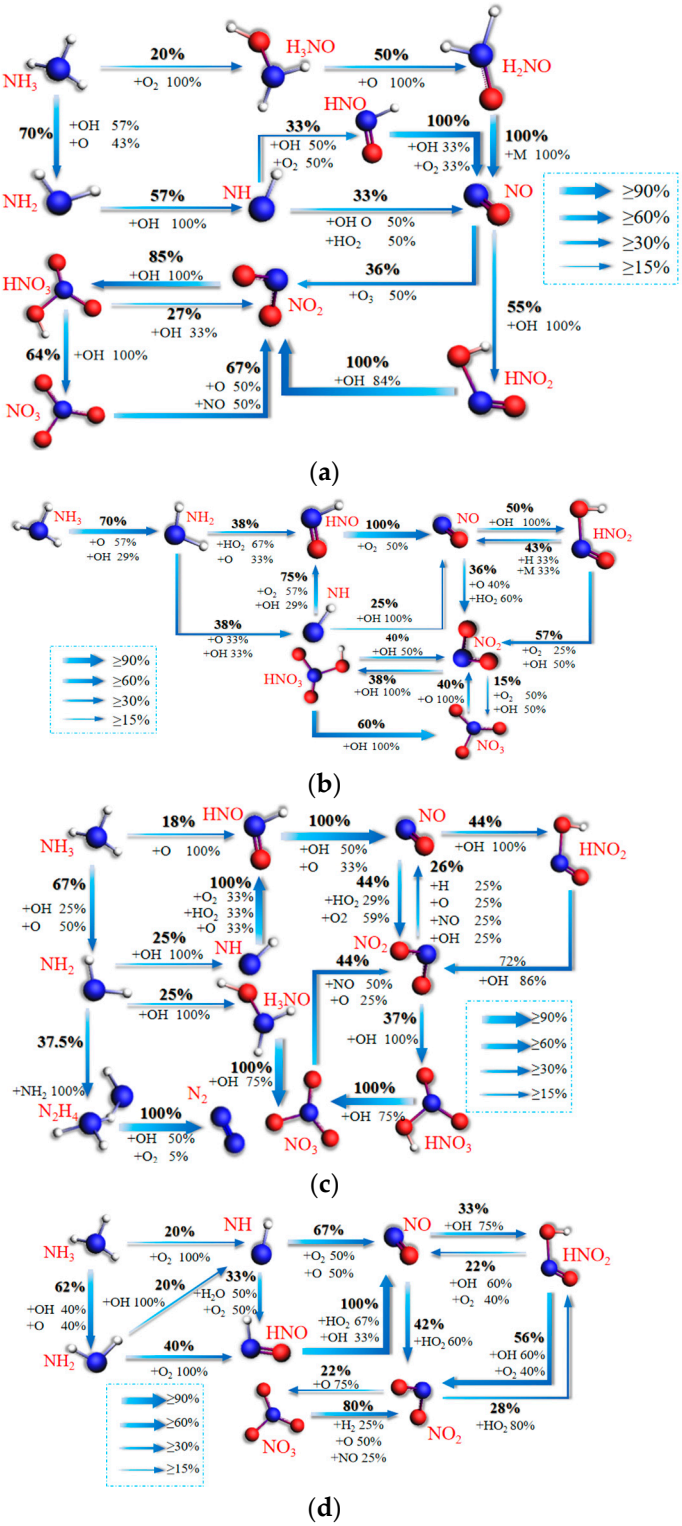

Figure 11. Mechanisms of NO_X formation from the blended combustion of ternary carbon-neutral fuels with different blending ratios. (**a**) 2:2:2; (**b**) 1:2:3; (**c**) 1:3:2; (**d**) 2:3:1.

Comparison of Figure 11a,b reveals that the main path of NO_X formation does not change much when the amount of NH_3 fuel is the same. The reaction path is simpler at 1:2:3 compared to the 2:2:2 blending ratio. The conversion ratio of NH_3 to NO also increases from 36.3% to 53.2%. This indicates that CH_4O makes the NH_3 reaction path simpler and NO_X formation easier. This is consistent with the conclusion in Section 3.2

that CH_4O promotes NH_3 combustion. Comparison of Figure 11a,c reveals that when the amount of CH_4O fuel is certain, the proportion of NH_3 is greater in the case of the ratio 1:3:2, which increases the reaction of NiHi to produce N_2 and NO_3. The conversion of NH_3 to NO_X increases from 36.3% to 51.5%. The conclusion that NO_X is mainly determined by NH_3 is confirmed. This conclusion is similarly confirmed in the comparative analysis of Figure 11a,d. The 2:3:1 pathway is simpler when the number of H_2 fuels is the same. The conversion of NH_3 to NO does not require a stepwise dehydrogenation reaction, and the conversion efficiency is increased to 50.6%.

Figure 12a–d shows the network diagrams of CO_2 formation reaction paths during the combustion of ternary fuels with $H_2/NH_3/CH_4O$ blending ratios of 2:2:2, 1:2:3, 1:3:2, and 2:3:1. Figure 12a shows the main reaction paths for the formation of CO and CO_2 in blended combustion with a ratio of 2:2:2. CHO_2 collides with groups such as OH and O_2 to form CO_2. The CO and CO_3 formed by CO_2 in the presence of groups such as OH, O_2, and O ultimately flow back to CO_2. The CO_2 remains relatively stable in the form of an end product.

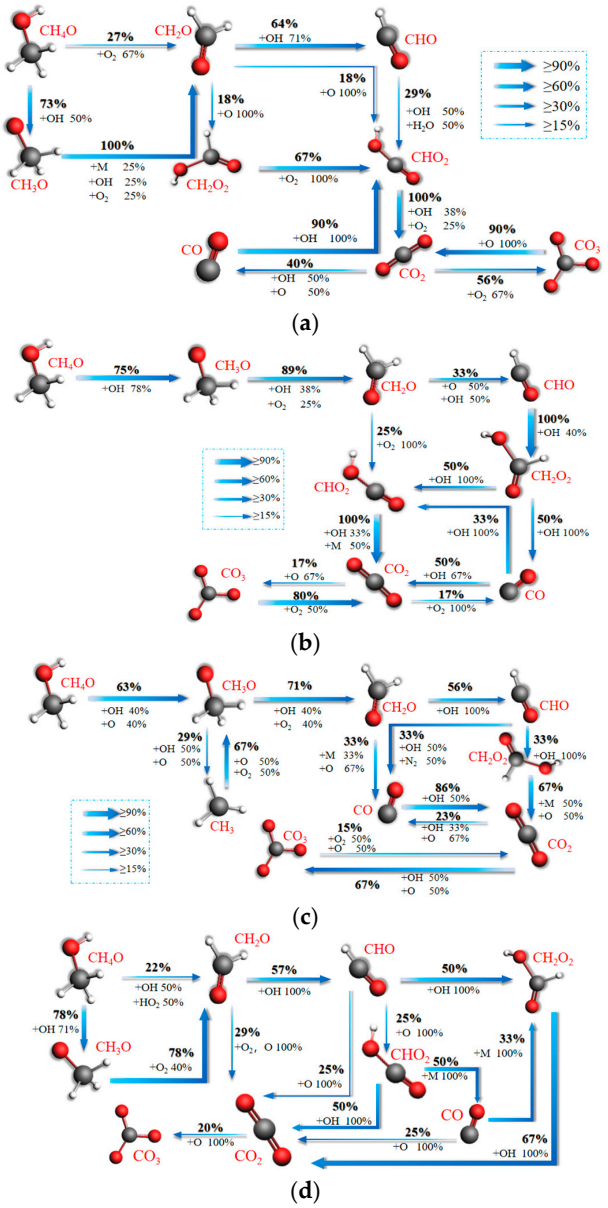

Figure 12. Mechanisms of CO and CO_2 formation in the blended combustion of ternary carbon-neutral fuels with different blending ratios. (**a**) 2:2:2; (**b**) 1:2:3; (**c**) 1:3:2; (**d**) 2:3:1.

Figure 12b represents the main reaction path for the formation of CO and CO_2 from blended combustion at a ratio of 1:2:3. It can be seen that CHO_2 collides with OH and other groups to generate CO_2. CO_2 is formed under the action of OH, O_2, O and other groups of CO and CO_3. Compared with the different times at 2:2:2, CH_2O_2 can collide directly with OH to generate CO at this ratio, and the reaction path is more complex.

Figure 12c shows the main reaction paths for CO and CO_2 formation in blended combustion when the ratio is 1:3:2. Overall, 33% of CH_2O collides with free radicals, such as O, to form CO; 56% of CH_2O collides with OH to form CHO; and the two portions of 33% of CHO collide with OH to form CH_2O_2 and CO, respectively.

Figure 12d shows the main reaction paths for CO and CO_2 formation from the combustion of ternary blends at a ratio of 2:3:1. It is found that 78% of CH_4O starts to react with OH and O to form CH_3O at the ratio of 2:3:1. Overall, 78% of CH_3O forms CH_2O in the presence of O_2; 57% of CH_2O collides with free radicals such as OH to form CHO; 29% of CH_2O collides with O_2 to form CO_2; and CHO generates CO and CO_2 directly or indirectly.

Comparison of Figure 12a,b shows that when the amount of NH_3 fuel is fixed, more CH_4O is converted to CH_2O with a ratio of 1:2:3 compared to 2:2:2. This may be due to the fact that H_2 promotes the oxidation of CH_4O. There were more reaction pathways for CO and CO_2 formation compared to the 2:2:2 ratio of 1:2:3. This may be caused by the high number of OH radicals in the reaction.

Comparison of Figure 12a,c reveals that the two paths do not differ much when the amount of CH_4O fuel is the same. This indicates that the reactions of CO and CO_2 during the combustion of ternary fuels are mainly influenced by CH_4O.

Comparison of Figure 12a,d reveals that when the number of H_2 fuels is the same, the path with a ratio of 2:3:1 is more complex. However, it does not mean that the oxidation of carbon-containing fuels in ternary fuels is more intense. Analyzing the percentage of oxidizing groups in the pathway reveals that, on the contrary, it is the oxidation of carbon-containing fuels at 2:3:1 that does not have enough O and OH groups. This time more intermediate OH groups are needed. From the analysis of OH groups mainly influenced by CH_4O it can be concluded that CO and CO_2 are mainly determined by CH_4O.

3. Materials and Methods

3.1. Reactive Force-Field Molecular Dynamics (ReaxFF MD)

ReaxFF MD combines molecular dynamics simulation with the calculation of reactive force fields. Its reactive force-field potential function is derived from experimental data and density functional theory, so the accuracy is close to quantum computation and does not require the predetermination of chemical reaction paths in the system [32]. ReaxFF is parameterized against QM-based training sets and is dependent on the bond order, while the bond order is a function of interatomic distance and updates at every iteration. Therefore, ReaxFF can describe bond formation and dissociation and provide highly accurate simulation results. ReaxFF MD has been widely used in the study of pyrolysis [33], combustion [34], explosions [35], oxidation [36], catalysis [37], and other systems involving physical chemistry. It provides a promising means of exploring the chemical behavior of complex molecular systems. Bond-order-dependent characterization is achieved by detailed parameterization of the atomic, bonding, angular, and torsional properties of each particle, and the interactions within the system [38]. The total energy of the system can be calculated by summing all partial energy terms as described in R1:

$$E_{system} = E_{bond} + E_{over} + E_{under} + E_{val} + E_{pen} + E_{tors} + E_{conj} + E_{vdWaals} + E_{coulomb} \quad (1)$$

where E_{bond}, E_{over}, E_{under}, E_{val}, E_{pen}, E_{tors}, and E_{conj} correspond to bond energy, over-coordination energy, under-coordination energy, bond angle energy, compensation energy, torsion energy, and four-body conjugation energy. The non-bonding terms mainly consist of van der Waals force energy ($E_{vdWaals}$) and Coulomb force energy ($E_{coulomb}$). When calculating non-bonding interactions, the charged atoms cross the truncation radius of the non-bonding interactions, thus leading to a jump in energy. Therefore, ReaxFF is

additionally corrected by introducing a seventh-order polynomial Taper function, which ensures that, at the truncation radius, the non-bonding interaction's first-, second-, and third-order derivatives of the energy term are all zero [39]. ReaxFF also takes better account of charge polarization by employing the electronegativity equalization method [40] and updates the atomic charges at each time step [41]. The detailed meaning of the ReaxFF parameters, the setup of the molecular structure, and the applicability of the reaction force field have been described in detail in a previous study [42].

3.2. Case Set-Ups

Table 1 lists all $H_2/NH_3/CH_4O$ blend combustion ReaxFF MD simulation cases in the high-pressure environment of this paper. The system density (ρ), equivalence ratio (φ), and simulation time are 0.05 g/cm^3, 0.5, and 1.25 ns, where more air (φ = 0.5) is used to ensure complete fuel combustion. Cases 1 to 5 represent the combustion of $H_2/NH_3/CH_4O$ blended fuel at 2000 K, 1000 K, 1500 K, 2500 K, and 3000 K. Cases 6 to 11 represent combustion at the same temperature with $H_2/NH_3/CH_4O$ ratios of 1:2:3, 1:3:2, 2:1:3, 2:3:1, 3:1:2, and 3:2:1. Three replicates with different initial configurations were simulated for individual cases. All the results reported in this work are ensemble-averaged from them. Through further comparative analysis, the mechanisms of CO, CO_2, and NO_X formation at different temperatures and fuel ratios are analyzed at the molecular level.

Table 1. ReaxFF MD cases of $H_2/NH_3/CH_4O$ blended combustion.

Case	H_2	NH_3	CH_4O	O_2	ρ, g/cm^3	T, K	φ
1	40	40	40	220	0.05	2000	0.5
2	40	40	40	220	0.05	1000	0.5
3	40	40	40	220	0.05	1500	0.5
4	40	40	40	220	0.05	2500	0.5
5	40	40	40	220	0.05	3000	0.5
6	20	40	60	260	0.05	2000	0.5
7	20	60	40	230	0.05	2000	0.5
8	40	20	60	250	0.05	2000	0.5
9	40	60	20	190	0.05	2000	0.5
10	60	20	40	210	0.05	2000	0.5
11	60	40	20	280	0.05	2000	0.5

3.3. Computational Details and Post-Processing

All the cases listed in Table 1 were analyzed in the ReaxFF module of AMS [43–45]. In this study, the HE2.ff force field [46] and the regular system with constant atomic number, volume, and temperature (NVT) were used. To ensure the overall stability of hydrocarbon fuel combustion, the energy and configuration of all simulated cases were first optimized using the "Geometry Optimization" and "Energy Optimization" plugins. Figure 13 shows the optimized systematic for Case 1, which shows that fuel and oxidant are uniformly blended, similar to a premixed flame, and similar to the cyclone burner we previously employed [47]. A Berendsen thermostat was used to control the temperature with a time step of 0.25 fs. Periodic boundary conditions were applied in all three xyz directions and the soot intermediate components and product distributions were analyzed from trajectories using a 0.3 Å bond level cutoff. All simulations were done on a server with an Intel(R) Xeon(R) Platinum 8352Y CPU @ 2.20 GHz, 64-core CPU, and 256 GB of RAM, and each set of conditions simulated for 1 ns required approximately 30 h of CPU time.

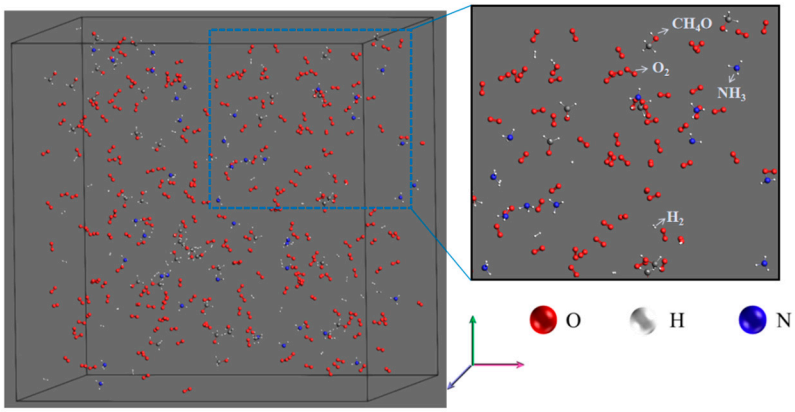

Figure 13. Optimization system for Case 1.

3.4. Validation of the ReaxFF MD Method

The reliability and validity of the ReaxFF MD method have been widely tested and verified in previous studies [38,39,48–51]. Among them, Wang et al. [39] constructed the reaction pathways in high-pressure combustion by tracking the trajectories of reacting atoms through ReaxFF MD to understand NO_X formation mechanisms in NH_3/CH_4 combustion at different temperatures and pressures. The results showed that a high temperature accelerated the rate of ammonia consumption, which was consistent with the experimental results. High pressure complicated the reaction pathway in NH_3/CH_4 combustion with the emergence of new intermediates and primitive reactions. In addition, they pointed out that ReaxFF MD is a valuable tool to reveal the underlying reaction mechanisms in combustion and pollutant formation. Liu et al. [51] investigated the chemical reactivity effects of NO on the oxidation of CH_4 using ReaxFF MD simulations and found that increasing the blending ratio of NO accelerated the rate of CH_4 consumption. This is mainly due to the fact that, on the one hand, conversion of NO to NO_2 generates OH radicals, which accelerates CH_4 consumption, while, on the other hand, NO can also inhibit CH_4 consumption by combining with reactive radicals. Wang et al. [48] applied ReaxFF MD and Py-GC/MS to investigate the characteristics of soot particulate formation in the process of the hydrogen-doped combustion of methane and ethylene. Both experimental and numerical results reflected that PAHs and ethylene were not the most important pollutants in the combustion process of CH_4. The experimental and numerical results reflect the evolution of PAHs and initial soot particles, as well as the different chemical effects of hydrogen doping on PAHs and soot formation.

4. Conclusions

In this paper, the effects of different reactant temperatures and blending ratios on combustion reaction rates and the formation characteristics of CO, CO_2, and NO_X in the combustion of $H_2/NH_3/CH_4O$ ternary carbon-neutral blended fuels were investigated for the first time using ReaxFF MD. The mechanisms of CO, CO_2, and NO_X formation in ternary blended fuels at different temperatures and blending ratios were investigated. The conclusions of this paper are summarized as follows:

(1) Heating accelerates the rate of H_2, NH_3, CH_4O, and O_2 consumption during ternary fuel combustion. However, the effect of heating on products such as N_2 and H_2O is not linear. The lowest amount of N_2 was produced and the most amount of NO_X was generated at 2000 K. The reaction rate and formation of CO and CO_2 increased with temperature. The CO peak shifted forward with increasing temperature. Free radical analysis revealed that CO, CO_2, and NO_X may be closely related to large amounts of OH. The predominant form present in NO_X changed with temperature. However, CO_2 has been the main form present in carbonaceous pollutants.

(2) Pollutant formation during the combustion of $H_2/NH_3/CH_4O$ ternary carbon-neutral blends was influenced by the coupling of H_2, NH_3, and CH_4O. NH_3 suppressed

the CO formation rate when the percentage of CH_4O was greater than 30%. However, the amount of CO and CO_2 formation was mainly determined by CH_4O, which increased the NH_3 combustion rate, causing NH_3 combustion to form more NO_X. In the ternary blended combustion process, NH_3 inhibits H_2 combustion, but CH_4O promotes H_2 combustion, in which NH_3 plays a major role.

(3) Analysis of the formation mechanisms of pollutants from the combustion of ternary carbon-neutral blended fuels at different temperatures reveals that high temperatures lead to more active oxidizing groups such as O in the reaction, which inhibits N_2 formation. The pathway of NO_X is more complicated at 2000 K. NO_X is formed by the conversion of NO. At low temperatures, half of the NO is oxidized directly to NO_3, but NO_2 and NO_3 cannot be reduced to NO directly. At 2000 K, NO needs to pass through NO_2 to form NO_3. A large amount of NO is oxidized to NO_2, and the reduction of NO_3 to NO_2 is higher. At high temperatures, the pathway to generate NO_3 disappears, and NO_2 has a higher reduction rate. Therefore, the main form of NO_X exists differently in different temperature states. Higher temperatures lead to the emergence of more CO formation paths, making CO and CO_2 be produced more quickly.

(4) By analyzing the formation mechanisms of pollutants in the combustion of ternary carbon-neutral blends with different blending ratios, it was found that CH_4O promotes the combustion of NH_3. This makes the reaction path simpler and easier for the generation of NO_X. CH_4O not only provides more carbon atoms involved in collisions for CO and CO_2 formation, but also leads to more OH and H formation. Therefore, the amount of CO and CO_2 formation is mainly determined by CH_4O.

Author Contributions: J.S.: investigation, data curation, visualization, analysis, writing—original draft, and writing—editing. Q.L.: investigation, data curation, and visualization. Y.W.: analysis, writing—review, and supervision. M.G.: writing—review and editing, supervision, project administration, and funding acquisition. X.H.: supervision and project administration. All authors have read and agreed to the published version of the manuscript.

Funding: This research was funded by the National Natural Science Foundation of China (52376008), the Natural Science Foundation of Anhui Province (2308085QE168), the University Synergy Innovation Program of Anhui Province (GXXT-2019-027), and the Funding for Postdoctoral Researchers' ScientificResearch Activities in Anhui Province (2023B718).

Institutional Review Board Statement: Not applicable.

Informed Consent Statement: Not applicable.

Data Availability Statement: Data are contained within the article.

Conflicts of Interest: The authors declare no conflict of interest.

Abbreviations

AMS	Amsterdam Modeling Suite	N_2	Nitrogen
CH_4O	Methanol	NH_3	Ammonia
CH_3O	Methoxy	NH_2	Ammonia radical
CH_2O	Formaldehyde	NO	Nitric oxide
CNG	Compressed natural gas	NO_2	Nitrogen dioxide
CO	Carbon monoxide	NO_3	Nitrogen trioxide
CO_2	Carbon dioxide	NOx	Nitrogen oxide
DGE	Diethylene glycol ether	NVT	Constant number of atoms, constant volume, and controlled temperature
H_2	Hydrogen	ReaxFF MD	Reactive molecular dynamics simulation
HC	Total hydrocarbons	PAH	Polycyclic aromatic hydrocarbons
HNO	Nitric acid	PM	Particulate matter
HO_2	Hydrogen peroxide radical	φ	Equivalent ratio
LNG	Liquefied natural gas	ρ	System density

References

1. Jisoo, S.; Sungwook, P. Numerical analysis for optimizing combustion strategy in an ammonia-diesel dual-fuel engine. *Energy Convers. Manag.* **2023**, *284*, 116980.
2. Zhang, L.; Sun, R.; Wang, Z.; Zhu, W.; Wang, X.; Qi, H. Application of experiments and density function theory on the formation mechanism of NH during O/Ar and O/HO combustion process of demineralized coals. *Fuel* **2023**, *331*, 125730. [CrossRef]
3. Chen, Z.; Li, P.; Anderson, R.; Wang, X.; Zhang, X.; Robison, L.; Redfern, L.R.; Moribe, S.; Islamoglu, T.; Gómez-Gualdrón, D.A.; et al. Balancing volumetric and gravimetric uptake in highly porous materials for clean energy. *Science* **2020**, *368*, 297–303. [CrossRef] [PubMed]
4. Yan, Z.; Yang, Y.; Li, Q.; Yan, Y.; Tian, Z.; Song, C.; Huang, Z. Study on effects of NH_3 and/or H_2 addition on the characteristics of soot formation and gas emissions in a laminar ethylene diffusion flame. *Fuel Process. Technol.* **2023**, *242*, 107633. [CrossRef]
5. Xuan, J.; He, L.; Wen, W.; Feng, Y. Hydrogenase and Nitrogenase: Key Catalysts in Biohydrogen Production. *Molecules* **2023**, *28*, 1392. [CrossRef] [PubMed]
6. Wang, Y.; Gu, M.; Zhu, Y.; Cao, L.; Zhu, B.; Wu, J.; Lin, Y.; Huang, X. A review of the effects of hydrogen, carbon dioxide, and water vapor addition on soot formation in hydrocarbon flames. *Int. J. Hydrogen Energy* **2021**, *46*, 31400–31427. [CrossRef]
7. Zhang, F.; Li, S.; Liu, Q.; Sun, J.; Wei, X.; Gu, M.; Wang, Y.; Huang, X. Effect of ammonia on the soot surface characteristics in ammonia/ethylene co-flow diffusion flames. *Fuel* **2023**, *341*, 127633. [CrossRef]
8. Dimitriou, P.; Javaid, R. A review of ammonia as a compression ignition engine fuel. *Int. J. Hydrogen Energy* **2020**, *45*, 98–118. [CrossRef]
9. Emir, E.; Yasin, A. Evaluation of ammonia fueled engine for a bulk carrier in marine decarbonization pathways. *J. Clean. Prod.* **2022**, *379*, 134688.
10. Sanchez, A.; Castellano, E.; Martín, M.; Vega, P. Evaluating ammonia as green fuel for power formation: A thermo-chemical perspective. *Appl. Energy* **2021**, *293*, 116956. [CrossRef]
11. Fenghour, A.; Wakeham, A.; Vesovic, V.; Watson, J.; Millat, J.; Vogel, E. The viscosity of ammonia. *J. Phys. Chem. Ref. Data* **1995**, *24*, 1649–1667. [CrossRef]
12. Frigo, S.; Gentili, R. Analysis of the behaviour of a 4-stroke Si engine fuelled with ammonia and hydrogen. *Int. J. Hydrogen Energy* **2013**, *38*, 1607–1615. [CrossRef]
13. Chai, W.; Bao, Y.; Jin, P.; Tang, G.; Zhou, L. A review on ammonia, ammonia-hydrogen and ammonia-methane fuels. *Renew. Sustain. Energy Rev.* **2021**, *147*, 111254. [CrossRef]
14. Zhang, R.; Chen, L.; Wei, H.; Li, J.; Chen, R.; Pana, J. Understanding the difference in combustion and flame propagation characteristics between ammonia and methane using an optical SI engine. *Fuel* **2022**, *324*, 124794. [CrossRef]
15. Nozari, H.; Karabeyouglu, A. Numerical study of combustion characteristics of ammonia as a renewable fuel and establishment of reduced reaction mechanisms. *Fuel* **2015**, *159*, 223–233. [CrossRef]
16. Charles, L.; Pierre, B.; Francesco, C.; Christine, M. Experimental investigation on ammonia combustion behavior in a spark-ignition engine by means of laminar and turbulent expanding flames. *Proc. Combust. Inst.* **2021**, *38*, 5859–5868.
17. Qi, Y.; Liu, W.; Liu, S.; Wang, W.; Peng, Y.; Wang, Z. A review on ammonia-hydrogen fueled internal combustion engines. *eTransportation* **2023**, *18*, 100288. [CrossRef]
18. Wang, S.; Li, Y.; Lv, J.; Liu, Z.; Gao, S.; Hu, J.; Zhang, J.; Zhong, W.; Zhao, Z. Evaluation of hydrogen addition on combustion and emission characteristics of dual-fuel diesel engines with different compression ratios. *Processes* **2023**, *11*, 2675. [CrossRef]
19. Caneon, K.; Mayank, M. Review on the production and utilization of green ammonia as an alternate fuel in dual-fuel compression ignition engines. *Energy Convers. Manag.* **2022**, *251*, 114990.
20. Wang, W.; Herreros, J.; Tsolakis, A.; York, A. Ammonia as hydrogen carrier for transportation; investigation of the ammonia exhaust gas fuel reforming. *Int. J. Hydrogen Energy* **2013**, *38*, 9907–9917. [CrossRef]
21. Alam, M.; Goto, S.; Sugiyama, K.; Kajiwara, M.; Mori, M.; Konno, M.; Motohashi, M.; Oyama, K. Performance and emissions of a DI diesel engine operated with LPG and ignition improving additives. *SAE Int. J. Engines* **2001**, *1*, 3680.
22. Miller, J.; Nagarajan, G.; Renganarayanan, S. LPG fueled diesel engine using diethyl ether with exhaust gas recirculation. *Int. J. Therm. Sci.* **2008**, *47*, 450–457. [CrossRef]
23. Karabektas, M.; Ergen, G.; Hosoz, M. The effects of using diethylether as additive on the performance and emissions of a diesel engine fuelled with CNG. *Fuel* **2014**, *115*, 855–860. [CrossRef]
24. Wang, Z.; Li, L. Effects of different ethanol/diesel blending ratios on combustion and emission characteristics of a medium-speed diesel engine. *Processes* **2022**, *10*, 173. [CrossRef]
25. Feng, H.; Chen, X.; Sun, L.; Ma, R.; Zhang, X.; Zhu, L.; Yang, C. The effect of methanol/diesel fuel blends with co-solvent on diesel engine combustion based on experiment and exergy analysis. *Energy* **2023**, *282*, 128792. [CrossRef]
26. Wang, W.; Herreros, J.; Tsolakis, A.; York, A. Reducing CO_2 footprint through synergies in carbon-free energy vectors and low carbon fuels. *Energy* **2016**, *112*, 976–983. [CrossRef]
27. Li, M.; He, X.; Hashemi, H.; Glarborg, P.; Lowe, V.M.; Marshall, P.; Fernandes, R.; Shu, B. An experimental and modeling study on auto-ignition kinetics of ammonia/methanol mixtures at intermediate temperature and high pressure. *Combust. Flame* **2022**, *242*, 112160. [CrossRef]
28. Xu, H.; Wang, J.; Zhang, C.; Dai, L.; He, Z.; Wang, Q. Numerical study on laminar burning velocity of ammonia flame with methanol addition. *Int. J. Hydrogen Energy* **2022**, *47*, 28152–28164. [CrossRef]

29. Lu, M.; Dong, D.; Wei, F.; Long, W.; Wang, Y.; Cong, L.; Dong, P.; Tian, H.; Wang, P. Chemical mechanism of ammonia-methanol combustion and chemical reaction kinetics analysis for different methanol blends. *Fuel* **2023**, *341*, 127697. [CrossRef]
30. Yang, W.; Ranga, D.; Luo, K.; Thevenin, D. Direct numerical simulation of turbulent premixed ammonia and ammonia-hydrogen combustion under engine-relevant conditions. *Int. J. Hydrogen Energy* **2022**, *47*, 11083–11100. [CrossRef]
31. Hong, C.; Ji, C.; Wang, S.; Xin, G.; Wang, Z.; Meng, H.; Yang, J. An experimental study of various load control strategies for an ammonia/hydrogen dual-fuel engine with the Miller cycle. *Fuel Process. Technol.* **2023**, *247*, 107780. [CrossRef]
32. van Duin, A.; Dasgupta, S.; Lorant, F.; Goddard, W.A. ReaxFF: A reactive force field for hydrocarbons. *J. Phys. Chem. A* **2001**, *105*, 9396–9409. [CrossRef]
33. Liu, J.; Guo, X. ReaxFF molecular dynamics simulation of pyrolysis and combustion of pyridine. *Fuel Process. Technol.* **2017**, *161*, 107–115. [CrossRef]
34. Guo, F.; Cheng, X.; Zhang, H. ReaxFF molecular dynamics study of initial mechanism of JP-10 combustion. *Combust. Sci. Technol.* **2012**, *184*, 1233–1243. [CrossRef]
35. Hong, D.; Liu, L.; Huang, Y.; Zheng, C.; Guo, X. Chemical effect of H_2O on CH_4 oxidation during combustion in O_2/H_2O environments. *Energy Fuels* **2016**, *30*, 8491–8498. [CrossRef]
36. Chowdhury, A.; van Duin, A. Extension of the ReaxFF combustion force field toward syngas combustion and initial oxidation kinetics. *J. Phys. Chem. A* **2017**, *121*, 1051–1068.
37. Liu, B.; Lusk, M.; Ely, J. Reactive molecular dynamic simulations of hydrocarbon dissociations on Ni(111) surfaces. *Surf. Sci.* **2012**, *606*, 615–623. [CrossRef]
38. Wang, J.; Jiang, X.; Luo, K. Exploring reaction mechanism for ammonia/methane combustion via reactive molecular dynamics simulations. *Fuel* **2023**, *331*, 125806. [CrossRef]
39. Kwon, H.; Shabnam, S.; van Duin, A.; Xuan, Y. Numerical simulations of yield-based sooting tendencies of aromatic fuels using ReaxFF molecular dynamics. *Fuel* **2020**, *262*, 116545. [CrossRef]
40. Mortier, W.; Ghosh, S.; Shankar, S. Electronegativity equalization method for the calculation of atomic charges in molecules. *Cheminform* **1986**, *108*, 4315–4320. [CrossRef]
41. Chenoweth, K.; van Duin, A.; Goddard, W. ReaxFF reactive force field for molecular dynamics simulations of hydrocarbon oxidation. *J. Phys. Chem. A* **2008**, *112*, 1040–1053. [CrossRef] [PubMed]
42. Bhoi, S.; Banerjee, T.; Mohanty, K. Molecular dynamic simulation of spontaneous combustion and pyrolysis of brown coal using ReaxFF. *Fuel* **2014**, *136*, 326–333. [CrossRef]
43. Lele, A.; Kwon, H.; Ganeshan, K.; Xuan, Y.; van Duin, A. ReaxFF molecular dynamics study on pyrolysis of bicyclic compounds for aviation fuel. *Fuel* **2021**, *297*, 120724. [CrossRef]
44. Senda, T.; Yamada, Y.; Morimoto, M.; Nono, N.; Sogabe, T.; Kubo, S.; Sato, S. Analyses of oxidation process for isotropic pitch-based carbon fibers using model compounds. *Carbon* **2019**, *142*, 311–326. [CrossRef]
45. Wang, Y.; Gong, S.; Wang, H.; Li, L.; Liu, G. High-temperature pyrolysis of isoprenoid hydrocarbon p-menthane using ReaxFF molecular dynamics simulation. *J. Anal. Appl. Pyrol.* **2021**, *155*, 105045. [CrossRef]
46. Zhang, L.; Zybin, S.; van Duin, A.; Dasgupta, S.; GoddardIII, W. Carbon cluster formation during thermal decomposition of octahydro-1,3,5,7-tetranitro-1,3,5,7-tetrazocine and 1,3,5-Triamino-2,4,6-trinitrobenzene high explosives from ReaxFF reactive molecular dynamics simulations. *J. Phys. Chem. A* **2009**, *113*, 10619–10640. [CrossRef] [PubMed]
47. Lin, Q.; Jiang, Y.; Liu, C.; Chen, L.; Zhang, W.; Ding, J.; Li, J. Controllable NO emission and high flame performance of ammonia combustion assisted by non-equilibrium plasma. *Fuel* **2022**, *319*, 123818. [CrossRef]
48. Wang, Y.; Gu, M.; Zhu, Y.; Cao, L.; Wu, J.; Lin, Y.; Huang, X. Analysis of soot formation of CH_4 and C_2H_4 with H_2 addition via ReaxFF molecular dynamics and pyrolysis–gas chromatography/mass spectrometry. *J. Energy Inst.* **2022**, *100*, 177–188. [CrossRef]
49. Chen, Z.; Sun, W.; Zhao, L. High-temperature and high-pressure pyrolysis of hexadecane: Molecular dynamic simulation based on reactive force field (ReaxFF). *J. Phys. Chem. A* **2017**, *121*, 2069–2078. [CrossRef]
50. Senftle, T.P.; Hong, S.; Islam, M.; Kylasa, S.B.; Zheng, Y.; Shin, Y.K.; Junkermeier, C.; Engel-Herbert, R.; Janik, M.J.; Aktulga, H.M.; et al. The ReaxFF reactive force-field: Development, applications and future directions. *NPJ Comput. Mater.* **2016**, *2*, 15011. [CrossRef]
51. Liu, Y.; Zhang, X.; Ding, J. Chemical effect of NO on CH_4 oxidation during combustion in O_2/NO environments. *Chem. Phys. Lett.* **2019**, *727*, 59–65. [CrossRef]